Author/s:
Kim, S;Heath, DE;Lee, WH;Lee, YM;Kentish, SE

Title:
Thermally rearranged nanofibrous composite membranes for carbon dioxide absorption and stripping

Date:
2022-07-15

Citation:
Kim, S., Heath, D. E., Lee, W. H., Lee, Y. M. & Kentish, S. E. (2022). Thermally rearranged nanofibrous composite membranes for carbon dioxide absorption and stripping. Journal of Membrane Science, 654, https://doi.org/10.1016/j.memsci.2022.120518.

Persistent Link:
https://hdl.handle.net/11343/324531

Thermally Rearranged Nanofibrous Composite Membranes for Carbon Dioxide Absorption and Stripping

S. Kim [a], D. E. Heath [b], W.H. Lee [c], Y. M. Lee [c], S. E. Kentish [*a]

[a] Department of Chemical Engineering, The University of Melbourne, Parkville, VIC 3010, Australia

[b] Department of Biomedical Engineering, The University of Melbourne, Parkville, VIC 3010, Australia

[c] Department of Energy Engineering, College of Engineering, Hanyang University, Seoul 04763, Republic of Korea

Abstract

We develop thermally rearranged (TR) nanofibre membranes for the capture of CO_2 using membrane gas absorption. The porous nature of the electrospun nanofibre membranes and the hydrophobicity of the TR polymers provide ideal properties for both CO_2 absorption and stripping. The use of thermal rearrangement after fabricating the nanofibre composite structures (TR-NFM) also interconnects the nanofibres and greatly improves mechanical strength. Surface hydrophobicity is further increased by electrospraying of nanoparticles onto the nanofibre membrane surface to increase roughness (TR-NCM), leading to higher breakthrough pressures and stable CO_2 stripping performance for up to 270 h at 100 °C without membrane wetting. The TR-NFM and TR-NCM membranes both show an order of magnitude increase in CO_2 absorption flux compared to a standard polytetrafluoroethylene (PTFE) membrane, offering strong potential for commercial application.

Keywords

TR polymer; membrane contactor; electrospinning; CO_2 stripping; CO_2 absorption.

1. Introduction

As global greenhouse gas emissions continue to rise, the application of CO_2 capture from gas streams is becoming inevitable [1-6]. Solvent absorption has emerged as the preferred method for CO_2 separation for synthesis and natural gas purification. This process involves absorbing CO_2 from a gas mixture into a liquid within a packed column absorber unit and then releasing pure CO_2 under high temperature or low pressure in a regeneration column. In membrane gas absorption (MGA), porous membranes replace the packed columns, providing a smaller footprint and the opportunity for solvent regeneration at lower temperatures. A membrane contactor also provides much greater CO_2 selectivity than for gas separation membranes, since it exploits differences in the solubility of species within the solvent. The much higher solubility of CO_2 results in a highly energy efficient and effective system.

Within a membrane contactor, gas transport between the gas and liquid absorbent occurs at the membrane surface. The membrane must be sufficiently porous to allow gas diffusion, but these pores must remain filled with gas. If liquid solvent enters and fills the pores, the resistance to gas diffusion will increase dramatically. As most solvents are aqueous, hydrophobic membranes are essential for this purpose. Hydrophobic polymers including polypropylene (PP), polytetrafluoroethylene (PTFE) and polyvinylidene fluoride (PVDF) have been utilised for this purpose [7]. Modification of these polymers through post treatment, blending with other polymers, and structural changes to improve the porosity and hydrophobicity has effectively enhanced the CO_2 transport properties [8-11]. For instance, PTFE nanofibres prepared by emulsion electrospinning and sintering can be an attractive material for this application [11], but the nanofibrous morphology is difficult to control and the fabrication process is complicated due to the insolubility of PTFE in organic solvents. Similarly, PVDF nanofibre membranes prepared by electrospinning have been shown to improve the CO_2 transport [10]. However, the CO_2 flux declines with time due to partial membrane wetting. The

intrinsic hydrophobicity of PVDF is relatively low so that it cannot completely prevent solvent penetration in the pores. An additional layer of PVDF microparticles on the nanofibre can improve the hydrophobicity by increasing surface roughness [10], but this approach is limited by poor adhesion of the particles, which often delaminate from the surface during operation.

Despite the lack of optimised materials for membrane contactors with high CO_2 flux and long-term performance stability, pilot-scale trials for post-combustion CO_2 capture have successfully demonstrated the technology over the last several years using commercial hollow fibre modules [12-14]. As one example, the use of an ultrathin and dense layer of poly(dimethyl siloxane) on porous hollow fibres prevented wetting at pilot scale with continuous operation for 28 days [14], but the CO_2 flux was significantly lower than that of porous PP hollow fibres due to the additional membrane resistance from the dense layer. The development of an appropriate membrane material is required before a commercial-scale operation in CO_2 separation within a membrane contactor can be readily implemented.

Herein, we develop electrospun membranes made from thermally rearranged (TR) polymers for membrane gas absorption and stripping. A precursor polymer hydroxyl polyimide (HPI) is first electrospun to form a nanofibre structure. This structure is then treated at 400 °C to cause thermal rearrangement. The resulting rigid and planar polybenzoxazole structure results in ideal properties for membrane gas absorption including excellent hydrophobicity, chemical and thermal stability in harsh environments and facile processing of the precursor polymer [15-22]. We believe that this excellent hydrophobicity, greater than conventional polymers such as PP or PVDF, can lead to stable operation without pore wetting. Moreover, the facile processibility of the precursor polymer enables controlled fabrication for nanofibre membranes with uniform fibre diameter and morphology. Previously, these excellent properties have allowed TR polymer membranes to save significant energy and cost in

applications including membrane distillation, gas separation and energy harvesting [18-20], and similar properties can be readily deployed in membrane gas absorption.

TR composite membranes are also prepared by coating the electrospun membranes with HPI nanoparticles using electrospraying, prior to thermal rearrangement, to increase surface roughness and further prevent pore wetting. Unlike our previous trials with PVDF membranes [10], which resulted in detachment of the nanoparticles from the surface, the thermal treatment can interconnect the nanofibres and nanoparticles, providing excellent stability without particle detachment.

We confirm the outstanding CO_2 absorption and stripping performance of both types of TR membranes using an aqueous solution of potassium glycinate as a CO_2 solvent. The excellent hydrophobicity and structural stability of these novel membranes provides long-term, stable high performance, which can readily be applied for practical CO_2 separation applications.

2. Experimental

2.1. Materials

The following reagents were of analytical grade and used as received: 4,4′-hexafluoroisopropylidene diphthalic anhydride (6FDA) and 3,3′-dihydroxyl-4-4′ diamino-biphenyl (HAB) from Central Glass (Tokyo, Japan); 2,4,6-Trimethyl-m-phenylenediamine (DAM), N-methyl-2-pyrrolidinone (NMP, 99.5%), *o*-xylene (98%), N,N-dimethylacetamide (DMAc, 99%), tetrahydrofuran (THF, 99.9%), 2-propanol (99.5%), sulfuric acid (H_2SO_4, 95%) and methyl orange (85%) from Sigma Aldrich (St Louis, MO); Glycine (98.5%) and potassium hydroxide (85%) from Thermo Fisher Co. (Waltham, MA). CO_2 (99.99%), N_2 (99.99%), argon (99.999%) and the CO_2/N_2 gas mixture (10/90 vol%, 99.99%) were supplied by the BOC Gas Company (North Ryde, Australia). A hydrophobic polytetrofluoroethylene (PTFE) membrane (11807 N, 0.2 μm) was purchased from Sartorius Stedim Biotech GmbH (Göttingen, Germany)

as a control. This is a commercially available membrane known for its strong hydrophobicity and high wetting resistance in long-term membrane gas absorption applications.

2.2. Synthesis of Precursor Polymers

The procedure for synthesising precursor polyimide is described in **Scheme 1**. Hydroxyl polyimide (HPI) was prepared by polycondensation of dianhydride and diamine, then imidization by azeotropic reaction [16, 20, 23, 24]. HAB (15 mmol) and DAM (15 mmol) were first completely dissolved in NMP (100 mL) and then 30 mmol of 6FDA was added to the solution. The reaction proceeded with vigorous stirring at 10 °C for 12 h under a nitrogen atmosphere to form hydroxyl poly(amic acid) solution. The azeotropic agent, *o*-xylene (60 mmol) was added to the solution, which was then stirred for 6 h under reflux at 180 °C to convert the amic acid groups to imide groups. The final HPI powder was obtained by precipitating in a methanol/water (1:3 v/v) mixture several times, then dried in a vacuum oven at 120 °C overnight.

2.3. Fabrication of nanofibre membranes

The HPI solution was dissolved in a mixture of DMAc and THF (1:1 w/w) at 27 wt% by vigorous stirring for 12 h at room temperature. The solution was then held for 24 h to remove any bubbles from the solution. An electrospinning device consisting of a single spray needle tip and a rotating steel drum collector (5 cm diameter and 15 cm length) was then used to fabricate HBI nanofibre membranes. The high voltage supply (Spellman CZE1000R, Hauppauge, NY) was attached to the needle tip at 12 kV and the collector at -4 kV respectively. The solution was fed to the needle tip at 1.5 mL h^{-1} through a syringe pump (Adelab Scientific, Thebarton, Australia). The rotation speed of the collector was controlled at 40 cm s^{-1} (150 rpm), with the distance between the tip and collector at 10 cm. A Linear Translation Stage (Thorlabs

Inc., Newton, NJ) was used to move the needle tip horizontally at a rate of 10 cm min^{-1}. A nanofibre freestanding mat, referred to as a nanofibre membrane (NFM), was prepared from 4.0 mL of the polymer solution. An additional 0.5 mL of 8 wt% HPI solution in DMAc/THF (5:5 w/w) was electrospun onto the NFM under the same conditions to obtain electrosprayed nanoparticles on the surface, referred to as a nanocomposite membrane (NCM). A heat roll laminator (J. Burrows) was then used to heat-press both the NFM and NCM membrane coupons at 110 °C.

2.4. Thermal rearrangement for thermally rearranged polybenzoxazole-co-polyimide (TR-PBOI) nanofibre membranes

The HPI nanofibre membranes were converted to polybenzoxazole-co-polyimide (PBOI) by a thermal rearrangement reaction within a tubular furnace under an argon atmosphere (STF1200 Tube Furnace, Across International, Livingston, NJ). The nanofibre membrane was located at the centre of the furnace and first heated to 300 °C for 1 h for residual solvent removal. The conversion to PBOI from HPI then occurred at 400 °C for 2 h.

2.5. Characterisation

Thermogravimetric analysis (TGA) was conducted to determine the thermal rearrangement conditions (TG 209 F1 Libra®, NETZSCH-Gerätebau GmbH, Selb, Germany). A scanning electron microscope was used to investigate the nanofibre morphology (SEM, FlexSEM, Hitachi, Tokyo, Japan), while the surface hydrophobicity of the membranes was investigated using a contact angle goniometer (OCA 20, DataPhysics Instruments, Filderstadt, Germany). Helium ion microscopy (HIM) was performed on an ORION NanoFab (Zeiss, Peabody MA) using a helium ion beam with a nominal beam current of 1.2 pA. A secondary electron signal was collected using an Everhart-Thornley (ET) detector, and images were

collected in line averaging mode, with typically 64 averages and a pixel dwell time of 0.5 µs. Charge neutralisation was performed in situ (the samples were not coated for imaging) using an electron flood gun, also operating in line mode.

A universal testing machine (Instron 5900 Series up to 50 N, Norwood, MA) was employed to determine the mechanical strength of three replicate specimens of each membrane according to the ASTM D638 standard. A dead-end filtration cell (HP4750, Sterlitech, Kent, WA) was used to measure the breakthrough pressure (p_B) measurement, but the solid end cap was changed to a mesh to allow observation of permeating water droplets. The applied pressure was increased in 5 kPa increments every 10 mins until water droplets were visible.

2.6. CO_2 Absorption and Stripping

A membrane contactor designed to accommodate a flat sheet membrane was used to investigate CO_2 absorption and stripping, as described in our previous work [10, 25]. The in-house manufactured stainless-steel membrane holder had an active membrane area of 14.6 cm^2 and was positioned in an oven for temperature control. During absorption experiments, the CO_2/N_2 (10:90 v/v) gas mixture was fed at a flow rate of 30 mL min^{-1} through the recessed gas channel. A sweep gas of pure N_2 was fed at the same flow rate for stripping experiments to remove the CO_2.

A magnetically driven mechanical stirrer (Heidolph Instruments, Model RZR 2020, Germany) was connected to the upper solvent chamber to minimise boundary layer mass transfer effects. The temperature of the convection oven was controlled between 25 and 50 °C for absorption and 60 and 100 °C for stripping. An aqueous solution of potassium glycinate (PG) of 30 wt% was prepared by mixing potassium hydroxide and glycine in a 1:1 molar ratio into purified water. The fresh solvent had a pH of 14, but this immediately declined as it started absorbing CO_2 from the CO_2/N_2 mixture during absorption experiments. A more stable state

was reached within 0.5-1.0 h and so the system was operated for 1 h before measurements were taken. For stripping, the solvent was pre-loaded by injecting CO_2 through the solution for 2 h, so that the solution pH was reduced to 10. This solvent was introduced to the solvent chamber at 60 mL min^{-1} using a peristaltic pump (Cole-Parmer, Vernon Hills, IL). The methods used to calculate Reynolds number, CO_2 flux, overall mass transfer coefficient and the membrane resistance are described in the Supplementary Material.

The membrane performance over longer timeframes was measured by continuous CO_2 stripping for 270 h at 100 °C, at gas and solvent flowrates of 30 and 60 mL min^{-1} respectively. To maintain a high CO_2 loading, pure CO_2 was bubbled into the solvent tank every 3 h.

3. Results and Discussion

Electrospinning/spraying is a method for readily fabricating nanofibres and particles of various size and morphology. This control over fibre and particle properties is achieved by tailoring the electrospinning parameters including electric field strength, solution conductivity, polymer concentration, system temperature and humidity. Ultrathin nanofibres with regular fibre diameter are preferred due to their high porosity and mechanical strength. However, unstable formation of the polymer solution jet, caused by an imbalance between viscoelastic, surface tension and electrostatic forces, often results in the generation of micron or nanometre size polymer particles instead of fibres.

In the present case, HPI (the precursor for the TR polybenzoxazole-*co*-polyimide (TR-PBOI) polymer) was first prepared by an azeotropic imidization method (Scheme 1). Then, the HPI membranes were fabricated by electrospinning in two distinct morphologies: a traditional nanofibre membrane (HPI-NFM) and a composite membrane with nanoparticles deposited on the surface of the nanofibre membrane (HPI-NCM) as illustrated in Fig. 1. The additional layer of the nanoparticles is expected to increase the hydrophobicity of the resulting membranes and

prevent pore wetting during operation due to the increased surface roughness. The electrospun HPI membranes were thermally rearranged at 400 °C under an argon atmosphere for 2 h to obtain the TR nanofibre membranes (TR-NFM and TR-NCM, respectively). TGA analysis confirmed the thermal rearrangement of the precursor polymers as described in Fig. 2. The first weight loss of HPI-NFM between 100 °C to 200 °C is evaporation of moisture absorbed in the nanofibres. The second loss between 400 °C to 450 °C is evolution of CO_2 molecules from the polymer during thermal rearrangement. The resulting TR-NFM has thermal stability up to 500 °C in an argon atmosphere.

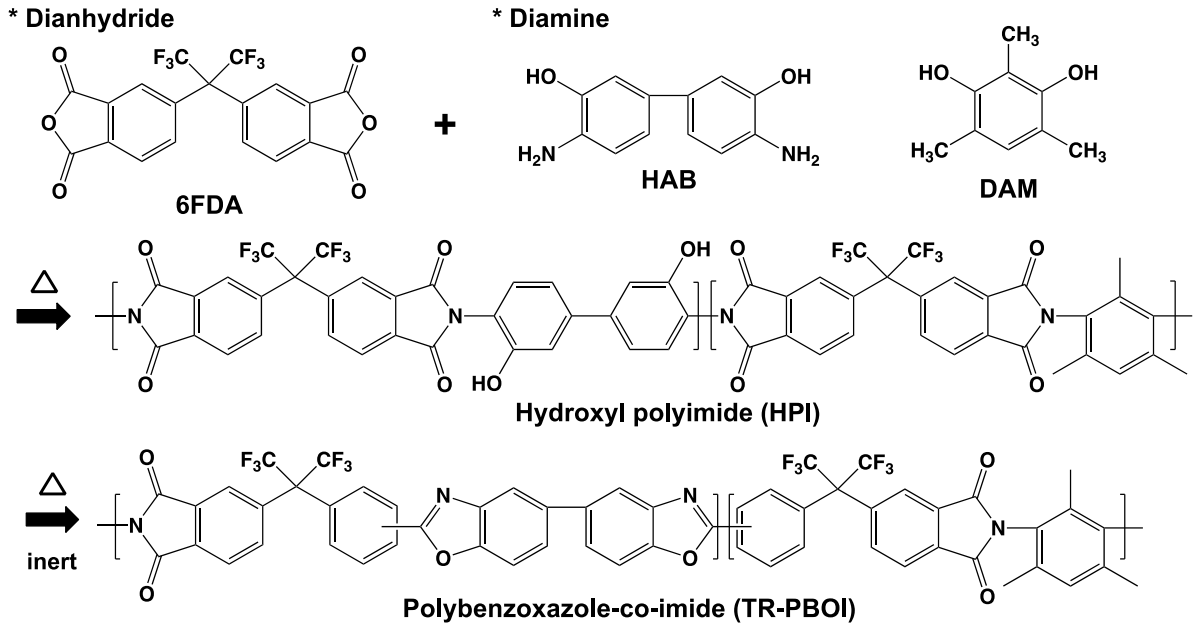

Scheme 1. Synthetic scheme for thermally arranged polybenzoxazole-co-polyimide (TR-PBOI).

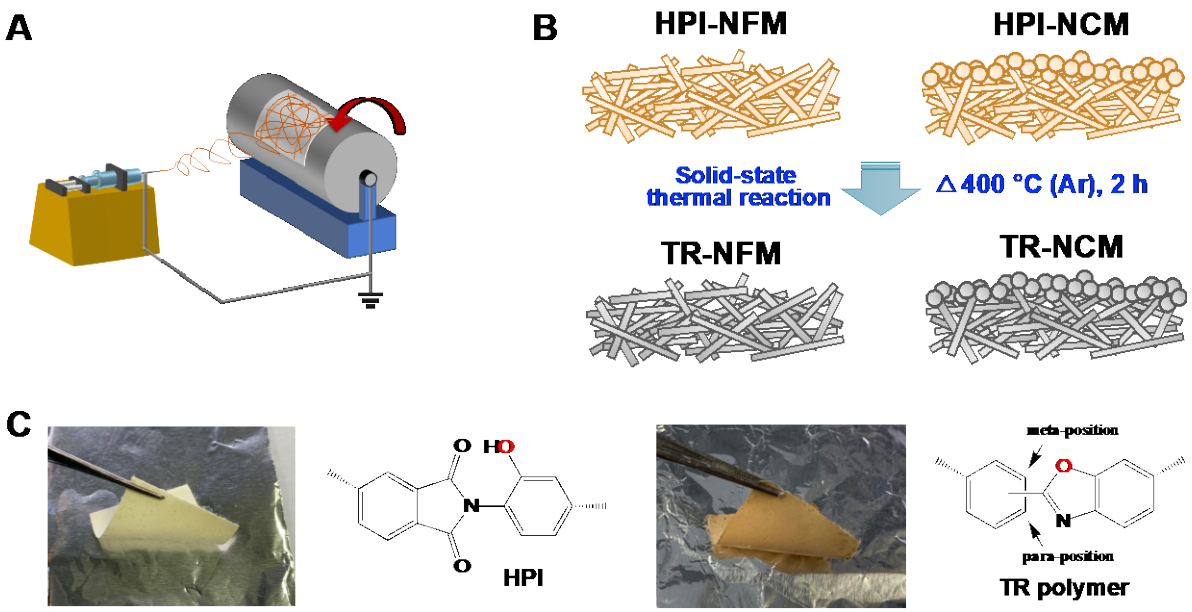

Fig. 1. Illustration of TR nanofibre membranes, showing (a) electrospinning procedure to fabricate nanofibres, (b) thermal reaction to prepare TR membranes from precursors, and (c) a photo and representative chemical structure of both the HPI precursor and resulting TR membranes.

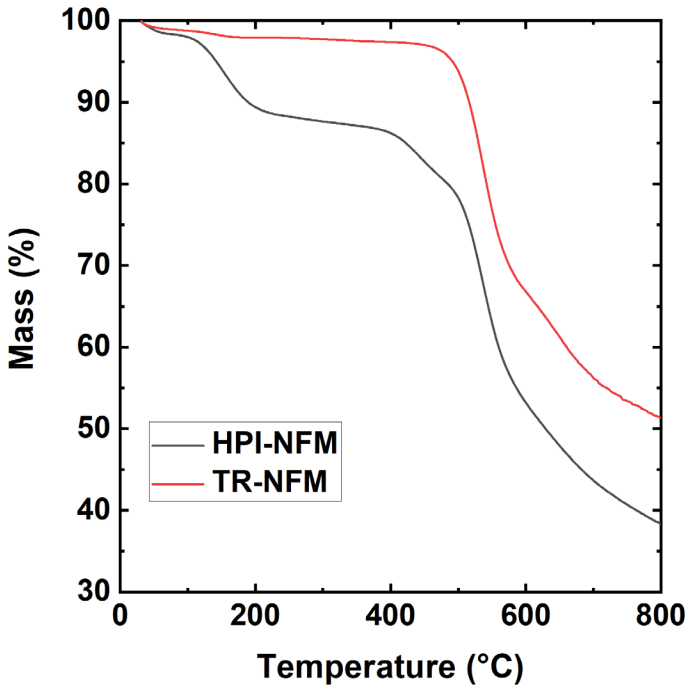

Fig. 2. Thermogravimetric analysis (TGA) of TR-PBOI and HPI nanofibre membranes.

The solution concentration is key to controlling the nanofibre morphology. Electrospinning of HPI solution of 8 wt%, 12 wt% and 27 wt% resulted in nanoparticles, bead-on-string and nanofibre morphologies, respectively, as observed by SEM images (Fig. 3). This membrane morphology, in terms of diameters of both nanofibres and nanoparticles, was unchanged by thermal re-arrangement for both the NFM and NCM (Fig. 4).

The TR membranes showed higher tensile strength (stress), but lower elasticity (strain at break) compared with the precursor HPIs due to their rigid polymer structures (Fig. 5). The nanofibres prepared with the 12 wt% solution (HPI-NFM 12% and TR-NFM 12%) were the weakest in mechanical strength, likely because of the small fibre diameters in the bead-on-string structures. The strength of both HPI and TR membranes then gradually increased with the solution concentration until 27 wt%. When the polymer concentration was increased to 30 wt%, the nanofibre diameter increased to around 1.2 μm, which led to slightly lower mechanical strength (stress) as previously observed [26-28]. Conversely, the nanofibres prepared with any concentration greater than 20 wt% showed similar strain at break. Nanofibre membranes (NFM) prepared from 27 wt% HPI were thus chosen for further study, giving a nanofibre diameter of 400 nm.

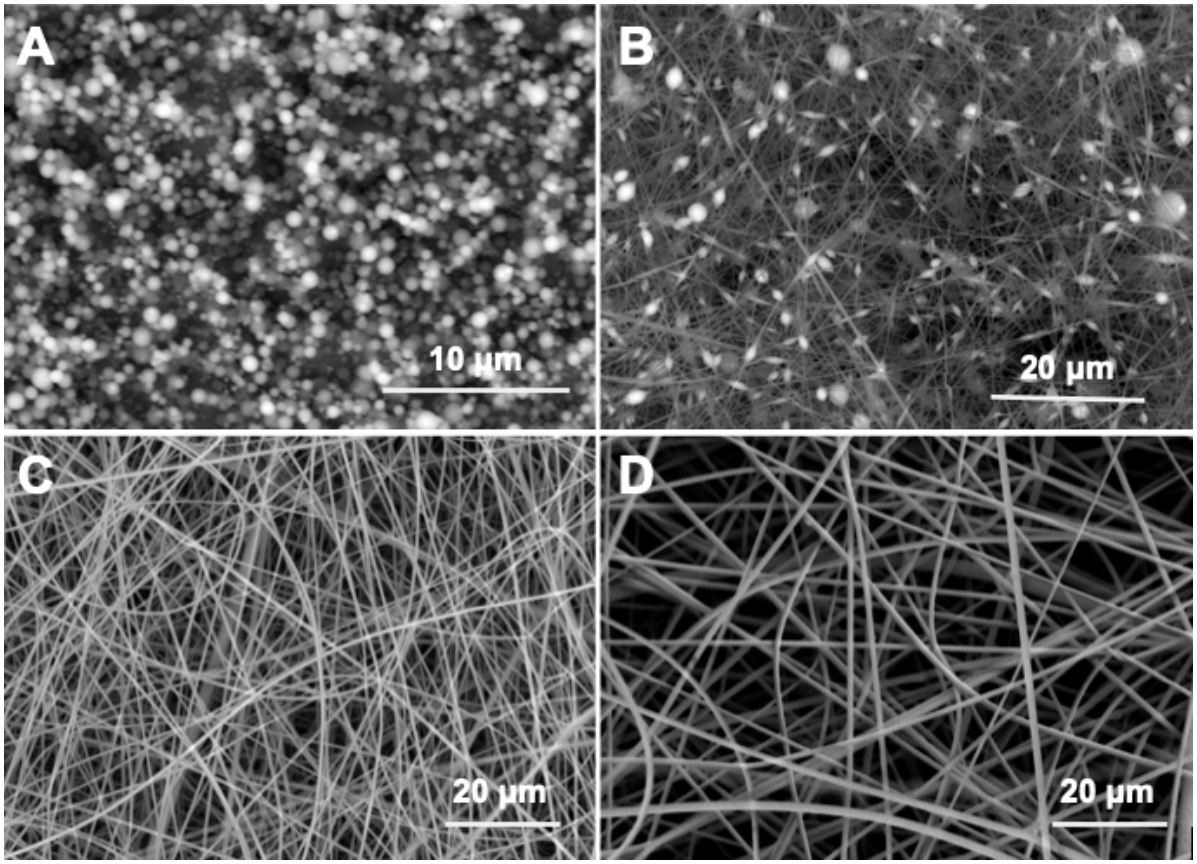

Fig. 3. SEM images of the nanofibre membrane surfaces when prepared from (a) 8 wt%, (b) 12 wt%, (c) 27 wt%, and (d) 30 wt% HPI solution.

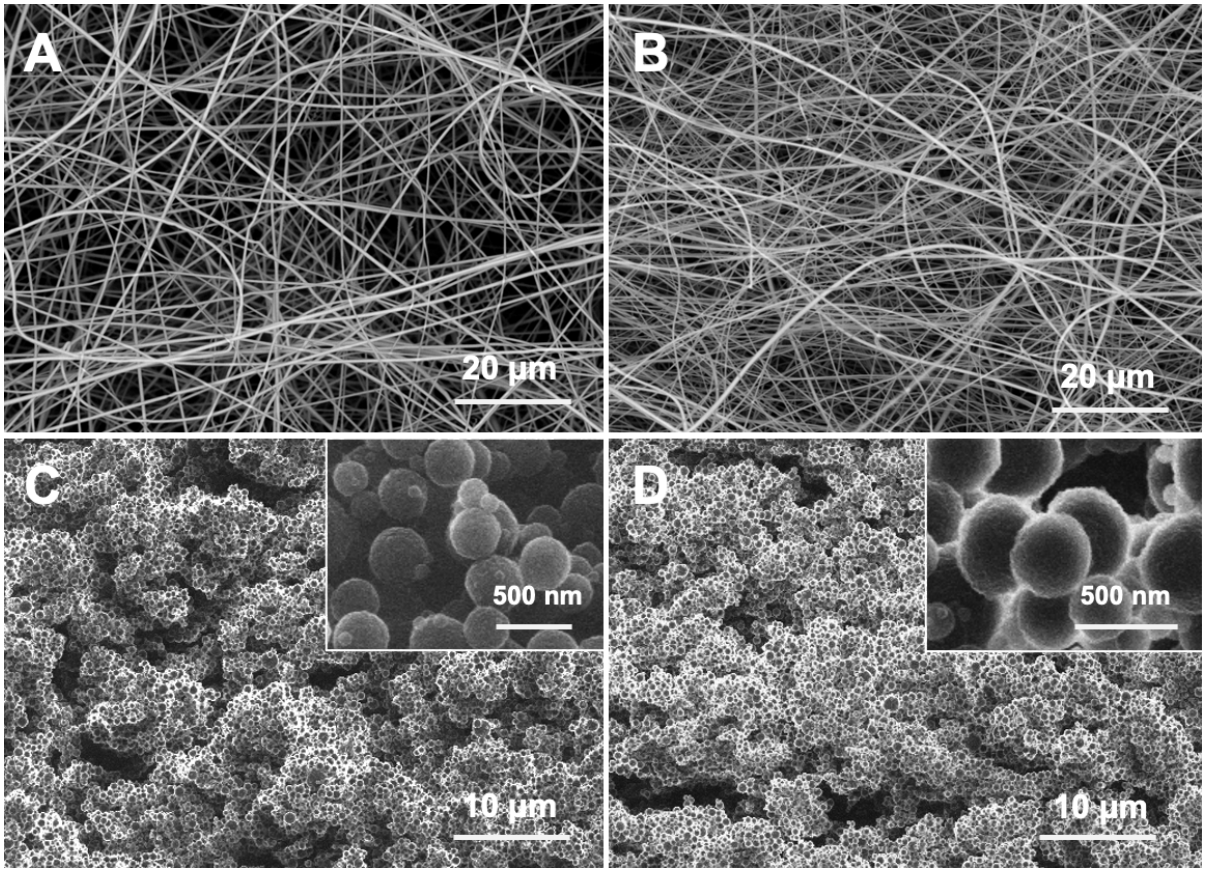

Fig. 4. SEM and HIM images of (a) HPI-NFM, (b) TR-NFM, (c) HPI-NCM, and (d) TR-NCM.

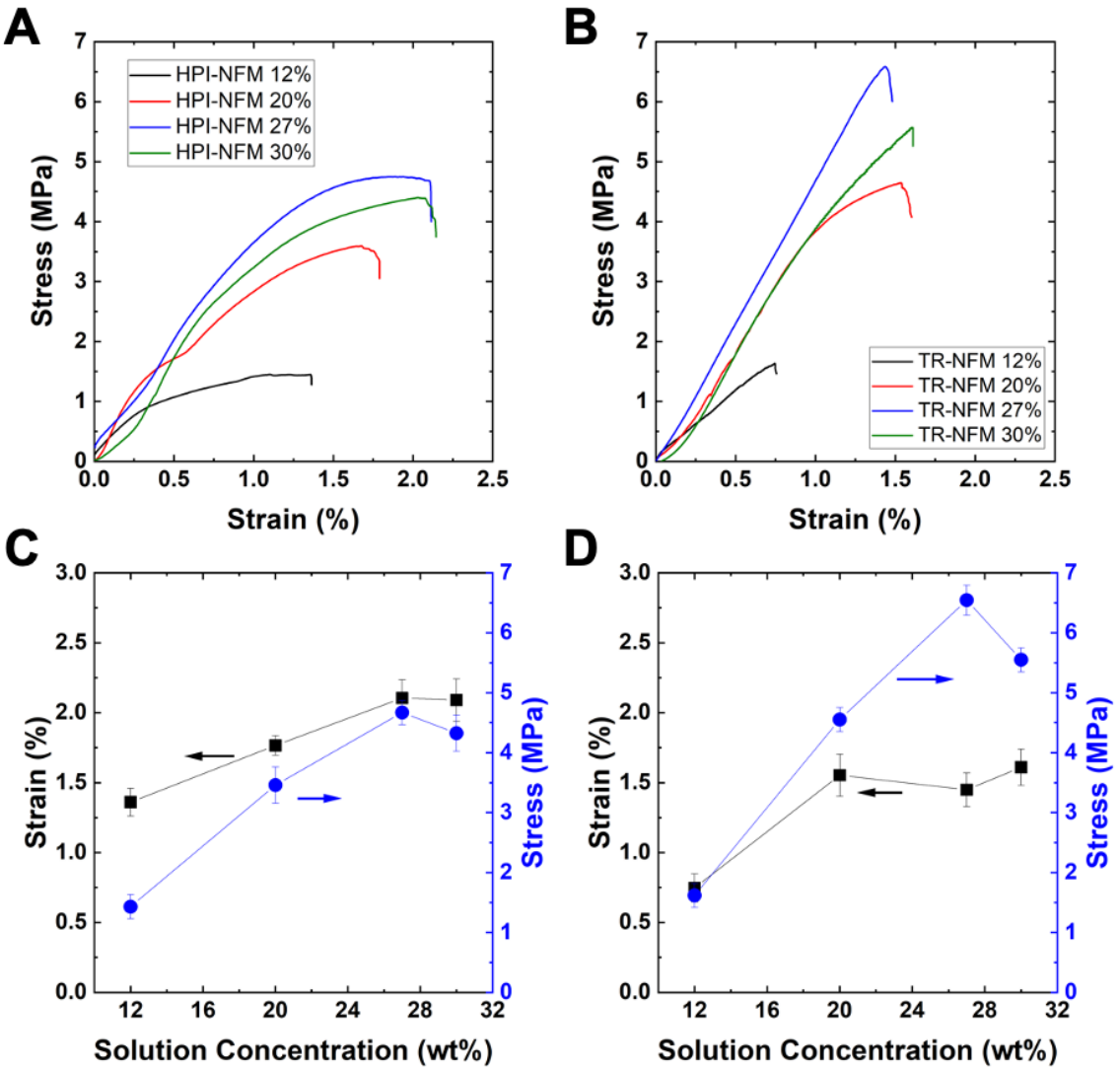

Fig. 5. Mechanical properties of nanofibre membranes as a function of HPI solution concentration: the stress-strain curves of (a) HPI-NFM and (b) TR-NFM, stress and strain at failure of (c) HPI-NFM and (d) TR-NFM as a function of solution concentration.

The thickness of a nanofibre membrane linearly increases as a function of the volume of the polymer solution loaded for membrane fabrication (Fig. 6a). The breakthrough pressure of the nanofibre also increases linearly to 112 kPa where 4 mL of the solution is loaded. This implies that the overlapping nanofibres generated during electrospinning fully cover the large pores in the membrane support. For both HPI-NFM and TR-NFM, the stress at break increased in a relatively linear manner with the volume of the electrospinning solution (Fig. 7), meaning that the increased membrane thickness also improved the mechanical strength. However, the

increase in the strain at break was less noticeable as this relates more to the extent of the entanglement between nanofibres. A loading of 4 ml, corresponding to a membrane thickness of 70 μm was chosen for further study to match the thickness of the commercial PTFE membrane (65 μm) that was used as a control, to fairly compare the membrane properties.

The layer of nanoparticles was deposited by electrospraying from an 8 wt% solution, resulting in nanoparticles with a diameter of 600 to 900 nm. To ensure that the nanoparticles covered the entire surface of the nanofibre mat, the breakthrough pressure of the composite membranes was monitored (Fig. 6b). This breakthrough pressure gradually increased, then reached equilibrium after 0.4 mL deposition. This means that most of the large pores on polybenzoxazole-co-polyimide surface was covered by the nanoparticles at this point. The thickness of the nanoparticle layer then gradually increased as the solution loading was increased between 0.5 to 1.0 mL. We chose 0.5 mL for fabrication of the nanofibre composite membranes (NCM) to ensure a layer of the nanoparticles without defects while minimising the membrane resistance from this additional layer.

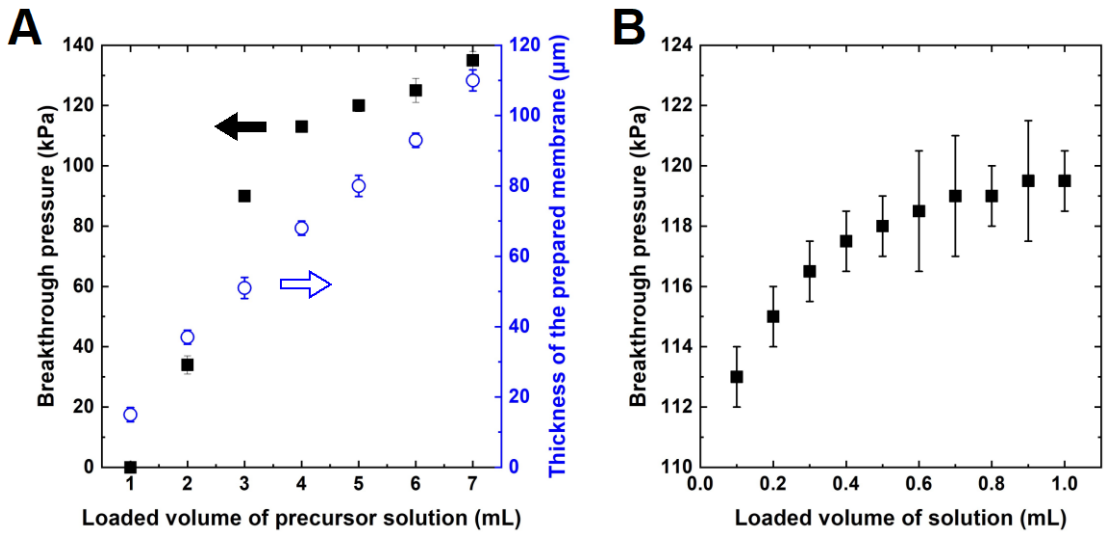

Fig. 6. Thickness and breakthrough pressure as a function of the (a) loaded solution volume of TR nanofibre membranes and (b) Electrosprayed solution volume for TR nanocomposite membranes.

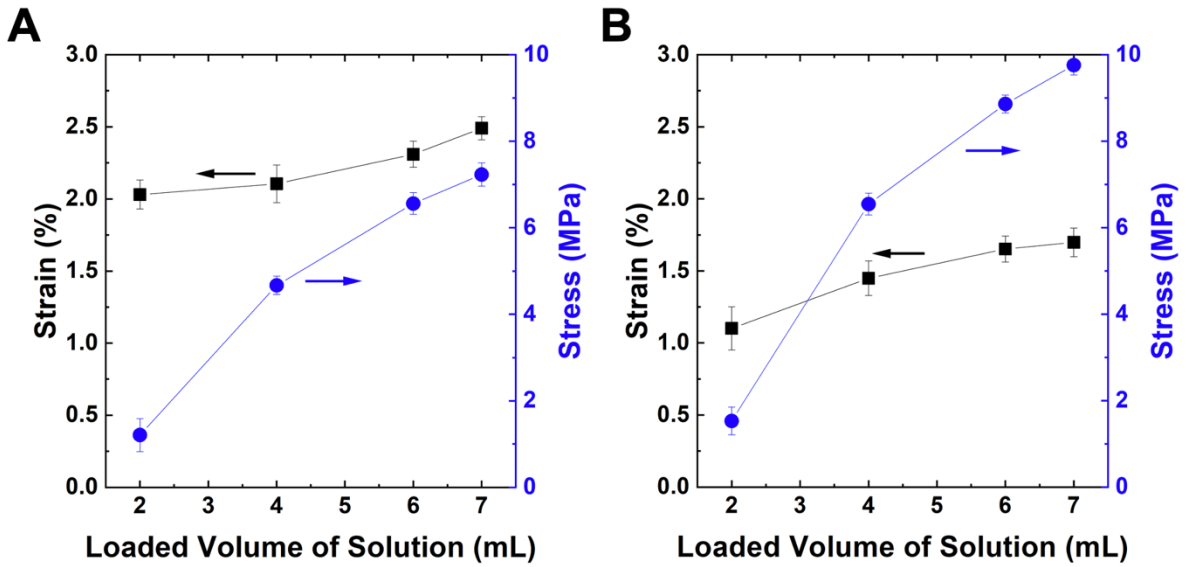

Fig. 7. Mechanical properties of (a) HPI-NFM and (b) TR-NFM as a function of loaded solution volume.

A hydrophobic surface is essential for a membrane contactor to generate CO_2 transport while preventing wetting. As shown in Fig. 8, the precursor HPI-NFM and HPI-NCM presented contact angles of 115° and 124°, respectively. The hydroxyl groups on the polyimide backbone impart hydrophilicity, although the nanofibrous and composite morphology increases the surface contact angle. After thermal rearrangement, these hydroxyl groups are eliminated. The new benzoxazole backbone has a low surface energy from its rigid and planar structure, resulting in improved hydrophobicity. TR-NFM and TR-NCM presented contact angles of 142° and 147°, respectively.

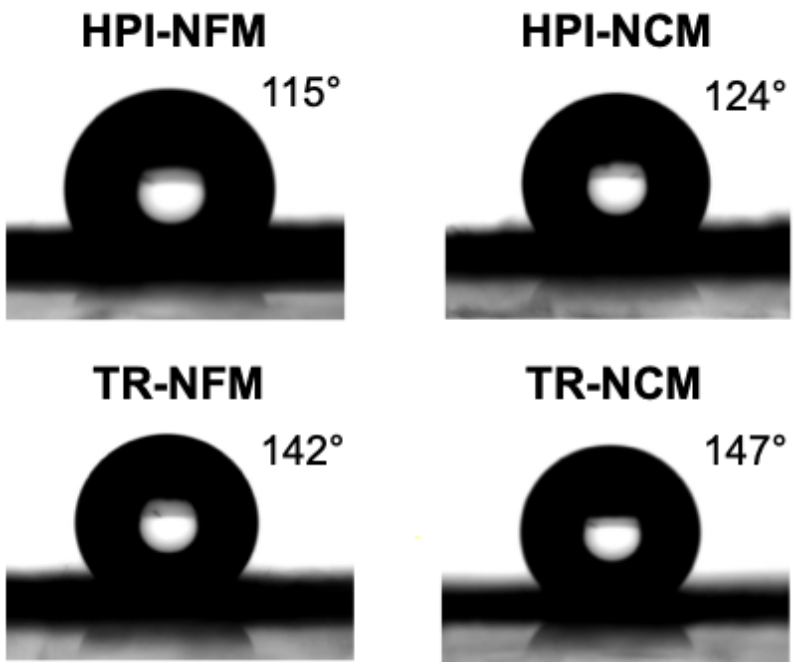

Fig. 8. Water contact angle of precursor and TR membranes.

Other properties of the nanofibre membranes such as porosity and breakthrough pressure are summarised in Table 1. The properties of a commercial PTFE asymmetric membrane are also included in this Table, as representative of a standard hydrophobic membrane. The overall porosity of the NFM and NCM slightly increased after thermal

rearrangement. This increase in overall porosity likely occurs to do the increase in free volume within the polymer matrix itself upon thermal rearrangement, as the overall morphology of the membrane fibres remains largely unchanged [16]. Both NFM and NCM possess similar porosity despite the additional coating layer on the NCMs because the nanofibrous substrate is the main factor to determine the overall porosity. The nanofibre membranes present much higher overall porosity than the PTFE asymmetric membrane at 32%, due to the overlapping nanofibre structures during fabrication. The water breakthrough pressure of the nanofibre membranes, at around 110 kPa, is comparable with other nanofibre membranes reported for membrane distillation applications, in the range of 25-200 kPa [18, 29-31]. Conversely, a breakthrough pressure of 200 kPa is recorded for the asymmetric PTFE membrane, which is related to the small pore size and porosity within the support structure. The maximum (d_{max}) and average ($d_{average}$) pore size within the membranes was characterised using the Young-Laplace Equation (Equation S1) and the Poiseuille and Knudsen mechanisms (Equation S2-S6). The pore sizes of both NFM and NCM were around the same after thermal rearrangement. NCM presented slightly smaller d_{max} and $d_{average}$ because of the TR nanoparticles coated on the surface, which fills the gap between the nanofibres. The porous structure required for effective molecular transport is evident from the effective surface porosity, which signals the connectivity of the pores throughout the membrane structure. HPI-NFM, HPI-NCM, TR-NFM and TR-NCM exhibited values of 154, 151, 160 and 158 m^{-1}, respectively, which is significantly greater than that of the asymmetric PTFE membranes at 111 m^{-1}. These TR nanofibre membranes with large pore sizes and effective surface porosity are thus highly advantageous for CO_2 transport during operations.

Table 1. Characteristics of the nanofibre and commercial PTFE membranes.

	HPI-NFM	**HPI-NCM**	**TR-NFM**	**TR-NCM**	**PTFE**
Membrane thickness (μm)	70 ± 2	72 ± 2	68 ± 1	70 ± 1	65 ± 1

Overall porosity (%)	76 ± 1	78 ± 1	79 ± 2	81 ± 2	32 ± 2
Water contact angle (°)	115 ± 1	124 ± 2	142 ± 1	147 ± 2	140 ± 1
Water breakthrough pressure (kPa)	105 ± 1	107 ± 2	113 ± 2	118 ± 1	200 ± 3
Contact angle of 2-propanol 20 wt% solution (°)	81 ± 1	81 ± 1	82 ± 1	82 ± 2	75 ± 2
Breakthrough pressure of 2-propanol 20 wt% solution (kPa)	47 ± 2	49 ± 1	41 ± 2	43 ± 1	101 ± 3
d_{max} (μm)	0.45	0.43	0.46	0.45	0.35
$d_{average}$ (μm)	0.42	0.41	0.43	0.41	0.23
Effective surface porosity (m^{-1})	154	151	160	158	111

The prepared membranes were tested in both CO_2 absorption and stripping using a membrane contactor apparatus. The in-house manufactured membrane holder was assembled with a membrane area of 14.6 cm^2. A magnetically driven stirrer was assembled within the upper solvent chamber to ensure turbulence and thus reduce the mass transfer resistance of the liquid layer above the membrane. An aqueous potassium glycinate (PG) solution was selected as a CO_2 absorbent. This is an attractive alternative solvent to alkanolamines such as monoethanolamine (MEA), diethanolamine (DEA), dimethylethanolamine (DMEA) or aminomethyl propanol (AMP) with its resistance to oxidative degradation as well as non-volatility and non-toxicity [32, 33]. Although MEA is the most commercially used solvent for CO_2 capture, MEA may not be suitable for membrane contactors since it easily degrades the membrane materials, requires a high regeneration energy and leads to solvent loss in the regeneration contactor due to its volatility [7]. PG is an amino acid that has similar CO_2 absorption properties to MEA [32]. It has been used for CO_2 separation in industrial processes such as BASF Alkazid and Siemens PostCap™ [34].

CO_2 absorption was investigated at between 25 to 50 °C using a CO_2/N_2 gas mixture in a volume ratio of 10:90, as a representative flue gas in post-combustion capture, with a gas flow rate at 30 mL min^{-1} and solvent flow rate at 60 mL min^{-1}. Fig. 9 describes the resulting CO_2 absorption flux and the overall mass transfer coefficient of the TR nanofibre and PTFE membranes as a function of Reynolds number, which is controlled by the rotation speed of the

stirrer in the solvent chamber. TR membranes exhibited an order of magnitude greater flux than PTFE membranes, as the high porosity, large pore sizes and small tortuosity of the nanofibres led to fast CO_2 transport. Between the two TR membranes, TR-NCM presented slightly lower absorption flux in all temperature ranges. Although TR-NCM has greater hydrophobicity than TR-NFM, the layer of the TR nanoparticles on the surface increased the mass transfer resistance. A gradual increase in the absorption flux was observed for all three membranes as the Reynolds number increased, which can be attributed to the reduction of mass transfer resistance within the solvent boundary layer. The increase in the absorption flux reached a plateau at Reynolds numbers above 2000, meaning that this liquid phase resistance was no longer significant. The increase in CO_2 absorption flux with temperature is also associated with the reduced resistance of the solvent boundary layer, due to the increased diffusivity of CO_2. A similar trend was observed in the overall mass transfer coefficients of the membranes. The CO_2 absorption flux of the TR nanofibre membranes was compared with other polymer membranes designed for MGA, as summarised in Table 2 [35-46]. Most of these membranes are commercial, or in-house prepared, hollow fibre membranes. As compared with these membranes, both TR-NFM and TR-NCM exhibited much higher absorption flux at 15.4 and 12.8 mmol m^{-2} s^{-1} at 25 °C.

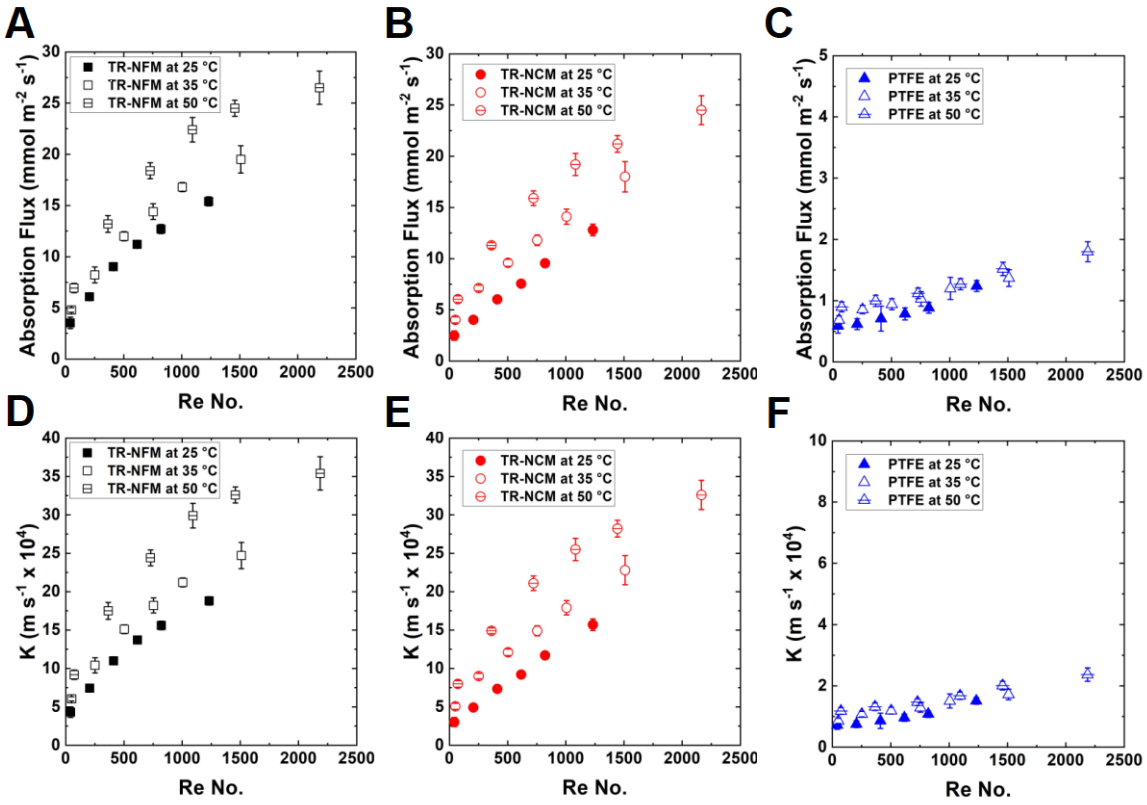

Fig. 9. The CO_2 absorption flux (a-c) and overall mass transfer coefficients (d-f) of TR nanofibre membranes and PTFE asymmetric membranes over a range of temperatures.

Table 2. A comparison of the CO_2 absorption flux for the membranes studied here with other literature reports. The temperature of measurement is not always available in these literature references but can usually be assumed to be ambient.

Membrane	Type	Absorbent	Feed gas (vol%)	Absorption flux (mmol m^{-2} s^{-1})	Ref.
TR-NFM at 25 °C	Nanofibre	PG 30 wt%	CO_2/N_2 (10/90)	15.4	Current study
TR-NFM at 50 °C	Nanofibre			26.5	
TR-NCM at 25 °C	Nanofibre			12.8	
TR-NCM at 50 °C	Nanofibre			24.5	
PDMS/PS	Nanofibre	AMP 1M	CO_2/N_2 (9/91)	1.9	[35]
PTFE	Hollow fibre	DMEA 2M	CO_2/Air (15/85)	1.8	[36]
PTFE	Hollow fibre	MEA 1M + PG 1M	CO_2/Air (15/85)	4.5	[37]
PVDF	Hollow fibre	DEA 1M	CO_2/N_2 (19/81)	0.6	[45]
PVDF-SiO_2	Hollow fibre	DEA 1M	CO_2/N_2 (19/81)	3.1	[38]
PVDF-ZMS5	Hollow fibre	DI water	Pure CO_2	6	[39]
PEI	Hollow fibre	DI water	Pure CO_2	0.88	[46]
PEI at 40 °C	Hollow fibre	MEA 1M	Pure CO_2	20	[40]
PVDF-fTiO_2	Hollow fibre	MEA 1M	Pure CO_2	11	[41]
PVDF-TiO_2-SiO_2	Hollow fibre	MEA 1M	Pure CO_2	8	[42]
PVDF-SiO_2-HDTMS	Hollow fibre	DEA 1M	CO_2/N_2 (19/81)	2.4	[43]
PP-fSiO_2	Hollow fibre	MEA 30 wt%	CO_2/CH_4 (20/80)	1.6	[44]

During stripping, the equilibrium CO_2 partial pressure, as well as the CO_2 diffusivity at the boundary layer increase with operating temperature, resulting in increased mass transfer. All three membrane samples exhibited this similar behaviour in mass transfer investigated between 60 to 100 °C (Fig. 10). The CO_2 stripping flux of all three membranes also gradually increased as a function of the liquid phase Reynolds number, which means that the pores on the membranes were gas-filled throughout the experimental conditions. Again, the increase in the overall mass transfer coefficient with temperature and Reynolds number (Fig. 11) is

associated with this reduction in boundary layer resistance. However, the TR nanofibre membranes presented much greater mass transfer coefficients than the PTFE membranes. A high Reynolds number is easily achieved during stripping, as the solvent viscosity (Table 3) is dramatically reduced at high temperature. The CO_2 stripping flux reached a steady state at Reynolds numbers above 2000, similar to the absorption flux. Again, the high CO_2 flux of TR nanofibre membranes is attributed to their hydrophobicity and porous structures, leading to fast molecular transport without causing surface wetting.

In membrane gas absorption, the overall mass transfer resistance (1/K) is affected by three resistances in series (liquid, membrane and gas phase, see Equation S10). The Wilson plot method can extract the membrane resistance from this overall mass transfer resistance through a correlation with the liquid phase Reynolds number (see Supplementary Information). This relationship is fitted in the region where the liquid phase resistance is rate controlling i.e., for Re < 2000 in the present case. The best fit of a straight line was found for a correlation between $1/K$ and $1/RE^{0.8}$ with R^2 between 0.9818 and 0.9993 (Fig. 10e). The y-intercept provides the combined mass transfer resistance of the membrane and gas phases. However, in membrane gas absorption, the gas phase resistance is marginal, so that this intercept predominantly indicates the membrane resistance [10], giving values of 69, 77, 720 s m^{-1} for TR-NFM, TR-NCM and PTFE, respectively. Fig. 10f illustrates the individual components of the overall, liquid and membrane mass transfer resistance at a Reynolds number at 1433. For all three membranes, most of the overall mass transfer resistance remains in the solvent boundary layer. However, for TR nanofibre membranes, the proportion of the resistance from this liquid phase is much greater, almost the same as the overall resistance, due to the small membrane resistance from their nanofibrous structures.

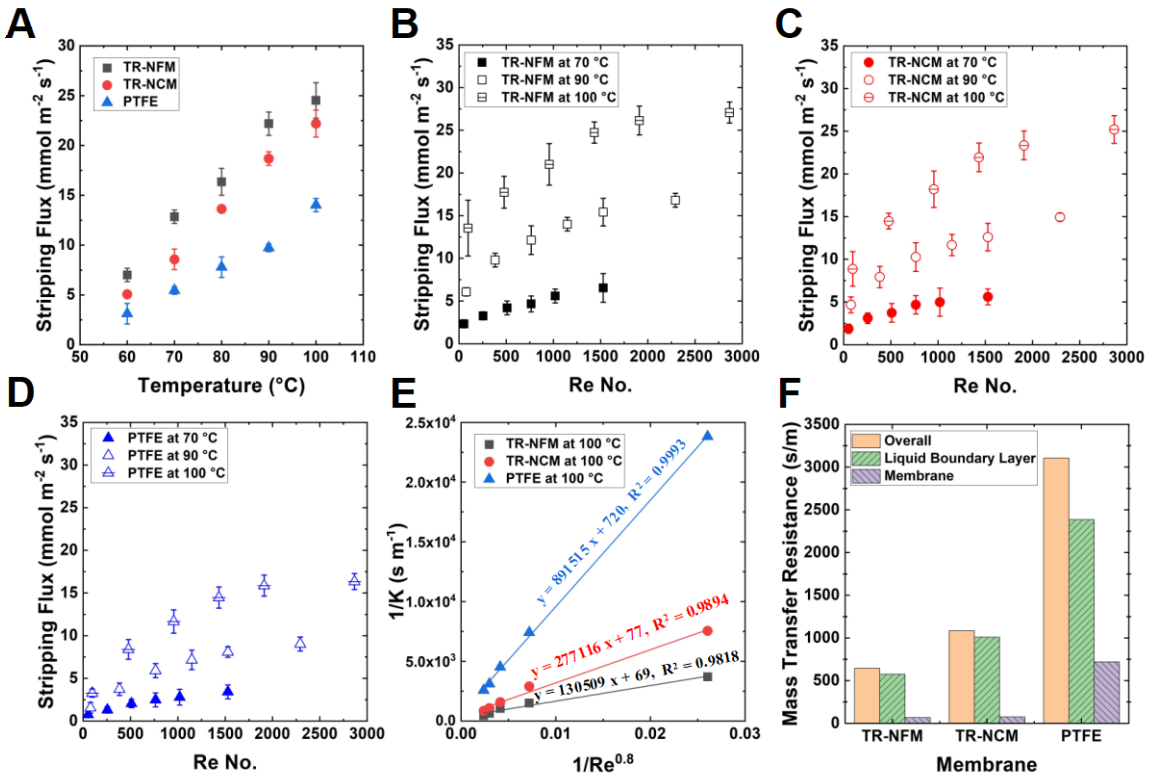

Fig. 10. The CO_2 stripping flux for both TR nanofibre and PTFE asymmetric membranes as a function of (a) operating temperature and (b-d) Reynolds Number. (e-f) Mass transfer resistance at a Reynolds number of 1433.

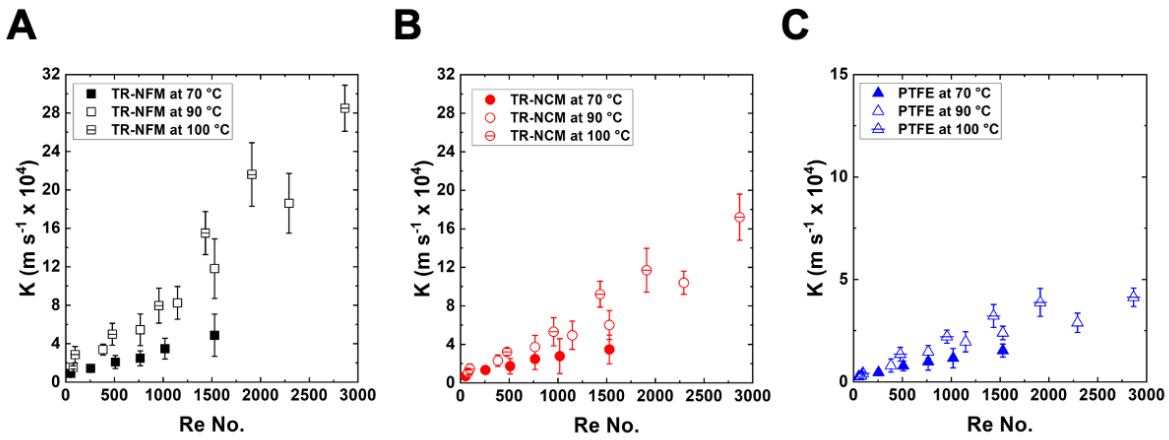

Fig. 11. Overall mass transfer coefficients of (a) TR-NFM, (b) TR-NCM, and (c) PTFE asymmetric membranes in CO_2 stripping.

Table 3. Viscosity of 30 wt% potassium glycinate aqueous solution as a function of temperature.

Temperature (°C)	Viscosity (kg m^{-1} s^{-1})
25	1.86×10^{-3}
35	1.52×10^{-3}
50	1.05×10^{-3}
70	9.0×10^{-4}
90	8.0×10^{-4}
100	7.0×10^{-4}

One of the most critical issues for membrane contactors is the flux stability. Most porous membranes applied to membrane absorption and stripping suffer from flux decline during long-term operation due to partial membrane wetting. As shown in Fig. 12, both TR-NFM and TR-NCM exhibited a high stripping flux during 270 h operation at 100 °C. All membranes experienced an inistial flux decline, but this stabilized after several hours. PTFE is known to be the only commercial polymer that can sufficiently prevent membrane wetting during membrane distillation or membrane gas absorption due its hydrophobicity and chemical stability, leading to constant flux with time. In the present case, however, this membrane suffers from its intrinsically lower permeability. The initial stripping flux of the TR-NFM was the highest at around 26 mmol m^{-2} s^{-1}. However, a greater flux decline was clearly observed, resulting from solvent penetration through the membrane pores by partial wetting, due to its high porosity and large pore sizes. On the other hand, the TR-NCM exhibited stable stripping over the same time span, confirming that the surface coating layer prevented membrane wetting even over a prolonged period at high temperature. Moreover, the TR nanoparticles remained securely fused to the nanofibre substrate during thermal rearrangement and did not detach from the composite structure over this period. The precursor hydroxyl polyimide is hydrophilic due to the hydroxyl groups on the polymer chain. The CO_2 stripping flux of these HPI-NFM membrane thus decreases to below 5.0 mmol m^{-2} s^{-1} within 60 h from its initial flux of 14 mmol m^{-2} s^{-1} due to membrane wetting by the aqueous solvent.

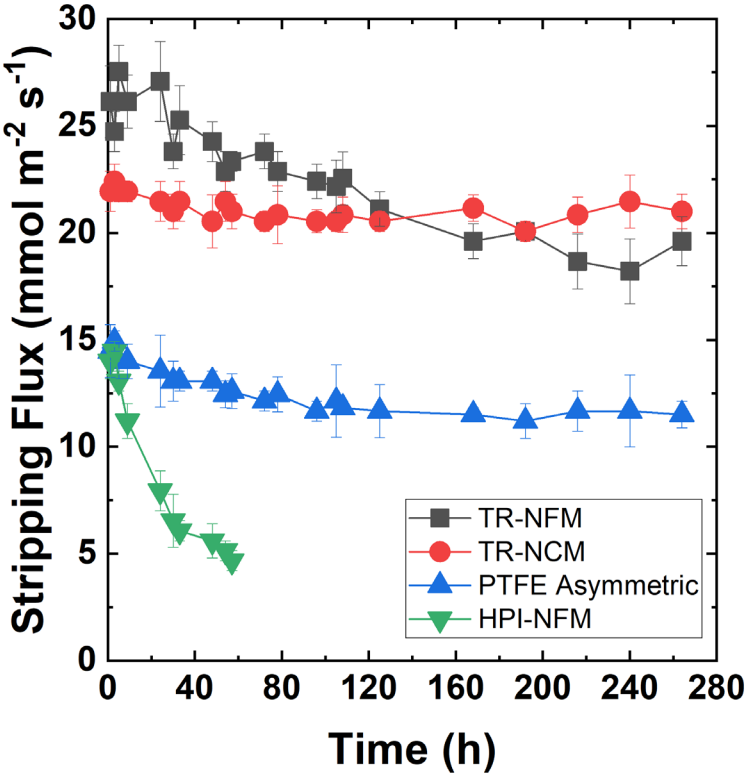

Fig. 12. Long-term gas flux of TR membranes in CO_2 stripping at 100 °C.

5. Conclusion

We have demonstrated the fabrication of TR nanofibrous membranes with robust, porous and hydrophobic morphology for CO_2 absorption and stripping. The ideal morphology was obtained by varying the electrospinning parameters, mainly solution viscosity, of the precursor HPI solution, to obtain both nanofibres and nanoparticle structures. The solid-state thermal rearrangement of HPI resulted in a stable attachment of the nanoparticle layers. Both the TR nanofibre membranes and composite membranes exhibited high CO_2 separation performance in a membrane contactor arrangement up to 50 °C for absorption and 100 °C for stripping, as compared with a standard PTFE membrane. In addition, TR nanoparticles on the surface enhanced the hydrophobicity by increasing surface roughness. In long term

experiments, the TR nanoparticles successfully prevented penetration of solvent into the nanofibres, resulted in a stable CO_2 stripping flux for up to 270 h. Notably, this fabrication method is easily scalable for possible commercial applications.

Acknowledgement

This work was funded by the Australian Research Council Discovery Projects Scheme (DP190102253). This work was performed in part at the Materials Characterisation and Fabrication Platform (MCFP) at the University of Melbourne and at the Victorian Node of the Australian National Fabrication Facility (ANFF).

Reference

[1] L. Liu, C.M. Doherty, E. Ricci, G.Q. Chen, M.G. De Angelis, S.E. Kentish, The influence of propane and n-butane on the structure and separation performance of cellulose acetate membranes, J. Membr. Sci., 638 (2021) 119677.

[2] J.G. Seong, W.H. Lee, J. Lee, S.Y. Lee, Y.S. Do, J.Y. Bae, S.J. Moon, C.H. Park, H.J. Jo, J.S. Kim, K.-R. Lee, W.-S. Hung, J.-Y. Lai, Y. Ren, C.J. Roos, R.P. Lively, Y.M. Lee, Microporous polymers with cascaded cavities for controlled transport of small gas molecules, Sci. Adv., 7 (2021) eabi9062.

[3] S.E. Kentish, 110th anniversary: process developments in carbon dioxide capture using membrane technology, Ind. Eng. Chem. Res., 58 (2019) 12868-12875.

[4] S. Kim, Y.M. Lee, Thermally rearranged (TR) polymer membranes with nanoengineered cavities tuned for CO_2 separation, Nanotechnology for Sustainable Development, (2012) 265-275.

[5] S. Kim, Membranes for Water, Gas and Ion Separation, Membranes, 11 (2021) 325.

[6] J. Kim, Q. Fu, K. Xie, J.M.P. Scofield, S.E. Kentish, G.G. Qiao, CO_2 separation using surface-functionalized SiO_2 nanoparticles incorporated ultra-thin film composite mixed matrix membranes for post-combustion carbon capture, J. Membr. Sci., 515 (2016) 54-62.
[7] S. Kim, C.A. Scholes, D.E. Heath, S.E. Kentish, Gas-liquid membrane contactors for carbon dioxide separation: A review, Chem. Eng. J., 411 (2021) 128468.
[8] X. Wu, B. Zhao, L. Wang, Z. Zhang, J. Li, X. He, H. Zhang, X. Zhao, H. Wang, Superhydrophobic PVDF membrane induced by hydrophobic SiO_2 nanoparticles and its use for CO_2 absorption, Sep. Purif. Technol., 190 (2018) 108-116.
[9] H. Pang, Z. Chen, H. Gong, M. Du, Fabrication of a super hydrophobic polyvinylidene fluoride–hexadecyltrimethoxysilane hybrid membrane for carbon dioxide absorption in a membrane contactor, J. Membr. Sci., 595 (2020) 117536.
[10] S. Kim, D.E. Heath, S.E. Kentish, Improved carbon dioxide stripping by membrane contactors using hydrophobic electrospun poly(vinylidene fluoride-co-hexafluoro propylene) (PVDF-HFP) membranes, Chem. Eng. J., 428 (2022) 131247.
[11] P. Zhao, N. Soin, K. Prashanthi, J. Chen, S. Dong, E. Zhou, Z. Zhu, A.A. Narasimulu, C.D. Montemagno, L. Yu, J. Luo, Emulsion Electrospinning of Polytetrafluoroethylene (PTFE) Nanofibrous Membranes for High-Performance Triboelectric Nanogenerators, ACS Appl. Mater. Interfaces, 10 (2018) 5880-5891.
[12] S. Li, D.J. Rocha, S. James Zhou, H.S. Meyer, B. Bikson, Y. Ding, Post-combustion CO_2 capture using super-hydrophobic, polyether ether ketone, hollow fiber membrane contactors, J. Membr. Sci., 430 (2013) 79-86.
[13] C.A. Scholes, A. Qader, G.W. Stevens, S.E. Kentish, Membrane Gas-Solvent Contactor Pilot Plant Trials of CO_2 Absorption from Flue Gas, Sep. Sci. Technol., 49 (2014) 2449-2458.

[14] C.A. Scholes, S.E. Kentish, A. Qader, Membrane gas-solvent contactor pilot plant trials for post-combustion CO_2 capture, Sep. Purif. Technol., 237 (2020) 116470.

[15] H.B. Park, C.H. Jung, Y.M. Lee, A.J. Hill, S.J. Pas, S.T. Mudie, E. Van Wagner, B.D. Freeman, D.J. Cookson, Polymers with cavities tuned for fast selective transport of small molecules and ions, Science, 318 (2007) 254-258.

[16] S. Kim, K.T. Woo, J.M. Lee, J.R. Quay, M.K. Murphy, Y.M. Lee, Gas sorption, diffusion, and permeation in thermally rearranged poly(benzoxazole-co-imide) membranes, J. Membr. Sci., 453 (2014) 556-565.

[17] S. Kim, Y.M. Lee, Rigid and microporous polymers for gas separation membranes, Prog. Polym. Sci., 43 (2015) 1-32.

[18] J.H. Kim, S.H. Park, M.J. Lee, S.M. Lee, W.H. Lee, K.H. Lee, N.R. Kang, H.J. Jo, J.F. Kim, E. Drioli, Thermally rearranged polymer membranes for desalination, Energy Environ. Sci., 9 (2016) 878-884.

[19] S. Kim, S.H. Han, Y.M. Lee, Thermally rearranged (TR) polybenzoxazole hollow fiber membranes for CO_2 capture, J. Membr. Sci., 403-404 (2012) 169-178.

[20] S. Kim, J. Hou, Y. Wang, R. Ou, G.P. Simon, J.G. Seong, Y.M. Lee, H. Wang, Highly permeable thermally rearranged polymer composite membranes with a graphene oxide scaffold for gas separation, J. Mater. Chem. A, 6 (2018) 7668-7674.

[21] W.H. Lee, J.G. Seong, J.Y. Bae, H.H. Wang, S.J. Moon, J.T. Jung, Y.S. Do, H. Kang, C.H. Park, Y.M. Lee, Thermally rearranged semi-interpenetrating polymer network (TR-SIPN) membranes for gas and olefin/paraffin separation, J. Membr. Sci., 625 (2021) 119157.

[22] Y. Lu, X. Hu, W.H. Lee, J.Y. Bae, J. Zhao, W. Nie, Z. Wang, J. Yan, Y.M. Lee, Effects of bulky 2,2′-substituents in dianhydrides on the microstructures and gas transport properties of thermally rearranged polybenzoxazoles, J. Membr. Sci., 639 (2021) 119777.

[23] H.J. Jo, C.Y. Soo, G. Dong, Y.S. Do, H.H. Wang, M.J. Lee, J.R. Quay, M.K. Murphy, Y.M. Lee, Thermally rearranged poly(benzoxazole-co-imide) membranes with superior mechanical strength for gas separation obtained by tuning chain rigidity, Macromolecules, 48 (2015) 2194-2202.

[24] S. Kim, H.J. Jo, Y.M. Lee, Sorption and transport of small gas molecules in thermally rearranged (TR) polybenzoxazole membranes based on 2,2-bis(3-amino-4-hydroxyphenyl)-hexafluoropropane (bisAPAF) and 4,4′-hexafluoroisopropylidene diphthalic anhydride (6FDA), J. Membr. Sci., 441 (2013) 1-8.

[25] J.A. Franco, S.E. Kentish, J.M. Perera, G.W. Stevens, Poly(tetrafluoroethylene) sputtered polypropylene membranes for carbon dioxide separation in membrane gas absorption, Ind. Eng. Chem. Res., 50 (2011) 4011-4020.

[26] A. Arinstein, E. Zussman, Electrospun polymer nanofibers: mechanical and thermodynamic perspectives, J. Polym. Sci. B Polym. Phys., 49 (2011) 691-707.

[27] M. Naraghi, S. Arshad, I. Chasiotis, Molecular orientation and mechanical property size effects in electrospun polyacrylonitrile nanofibers, Polymer, 52 (2011) 1612-1618.

[28] J. Pelipenko, J. Kristl, B. Janković, S. Baumgartner, P. Kocbek, The impact of relative humidity during electrospinning on the morphology and mechanical properties of nanofibers, Int. J. Pharm., 456 (2013) 125-134.

[29] L.D. Tijing, Y.C. Woo, W.-G. Shim, T. He, J.-S. Choi, S.-H. Kim, H.K. Shon, Superhydrophobic nanofiber membrane containing carbon nanotubes for high-performance direct contact membrane distillation, J. Membr. Sci., 502 (2016) 158-170.

[30] Y. Huang, Q.-L. Huang, H. Liu, C.-X. Zhang, Y.-W. You, N.-N. Li, C.-F. Xiao, Preparation, characterization, and applications of electrospun ultrafine fibrous PTFE porous membranes, J. Membr. Sci., 523 (2017) 317-326.

[31] S.H. Park, J.H. Kim, S.J. Moon, E. Drioli, Y.M. Lee, Enhanced, hydrophobic, fluorine-containing, thermally rearranged (TR) nanofiber membranes for desalination via membrane distillation, J. Membr. Sci., 550 (2018) 545-553.

[32] A.F. Portugal, J.M. Sousa, F.D. Magalhães, A. Mendes, Solubility of carbon dioxide in aqueous solutions of amino acid salts, Chem. Eng. Sci., 64 (2009) 1993-2002.

[33] E. Hosseini, G.W. Stevens, C.A. Scholes, Membrane gas-solvent contactors undergoing oscillating solvent flow for enhanced carbon dioxide capture, Sep. Purif. Technol., 227 (2019) 115653.

[34] G. Hu, K.H. Smith, Y. Wu, K.A. Mumford, S.E. Kentish, G.W. Stevens, Carbon dioxide capture by solvent absorption using amino acids: A review, Chin. J. Chem. Eng., 26 (2018) 2229-2237.

[35] Y.-F. Lin, W.-W. Wang, C.-Y. Chang, Environmentally sustainable, fluorine-free and waterproof breathable PDMS/PS nanofibrous membranes for carbon dioxide capture, J. Mater. Chem. A, 6 (2018) 9489-9497.

[36] F. Cao, H. Gao, Q. Xiong, Z. Liang, Experimental studies on mass transfer performance for CO_2 absorption into aqueous N,N-dimethylethanolamine (DMEA) based solutions in a PTFE hollow fiber membrane contactor, Int. J. Greenh. Gas Control., 82 (2019) 210-217.

[37] G. Gao, H. Gao, Z. Liang, Mass transfer performance and correlations for CO_2 absorption into aqueous blended PG/MEA in PTFE membrane contactor, J. Chem. Technol. Biotechnol., 95 (2020) 27-39.

[38] Z. Chen, Q. Shen, H. Gong, M. Du, Preparation of a novel dual-layer polyvinylidene fluoride hollow fiber composite membrane with hydrophobic inner layer for carbon dioxide absorption in a membrane contactor, Sep. Purif. Technol., 248 (2020) 117045.

[39] M. Rezaei-DashtArzhandi, A. Ismail, P. Goh, I. Wan Azelee, M. Abbasgholipourghadim, G. Ur Rehman, T. Matsuura, Zeolite ZSM5-filled PVDF hollow

fiber mixed matrix membranes for efficient carbon dioxide removal via membrane contactor, Ind. Eng. Chem. Res., 55 (2016) 12632-12643.

[40] R. Naim, A. Ismail, T. Matsuura, I. Rudaini, S. Abdullah, Polyetherimide hollow fiber membranes for CO_2 absorption and stripping in membrane contactor application, RSC Adv., 8 (2018) 3556-3563.

[41] Y. Lin, Y. Xu, C.H. Loh, R. Wang, Development of robust fluorinated TiO_2/PVDF composite hollow fiber membrane for CO_2 capture in gas-liquid membrane contactor, Appl. Surf. Sci., 436 (2018) 670-681.

[42] Y. Xu, Y. Lin, M. Lee, C. Malde, R. Wang, Development of low mass-transfer-resistance fluorinated TiO_2-SiO_2/PVDF composite hollow fiber membrane used for biogas upgrading in gas-liquid membrane contactor, J. Membr. Sci., 552 (2018) 253-264.

[43] H. Gong, H. Pang, M. Du, Z. Chen, Fabrication of a superhydrophobic mixed matrix PVDF-SiO_2-HDTMS hollow fiber membrane for membrane contact carbon dioxide absorption, Clean. Eng. Technol., 5 (2021) 100278.

[44] S. Raveshiyan, P. Amirabedi, R. Yegani, B. Pourabbas, A. Tavakoli, CO_2 absorption through PP/fSiO_2 nanocomposite hollow fiber membrane contactor, Polyolefins J., 9 (2022) 61-71.

[45] M. Du, H. Gong, H. Pang, Q. Shen, Z. Chen, Fabrication and characterization of poly (vinylidene fluoride)–polytetrafluoroethylene composite membrane for CO_2 absorption in gas–liquid contacting process, J. Appl. Polym. Sci., 136 (2019) 47767.

[46] M. Rahbari-Sisakht, A.F. Ismail, D. Rana, T. Matsuura, Effect of different additives on the physical and chemical CO_2 absorption in polyetherimide hollow fiber membrane contactor system, Sep. Purif. Technol., 98 (2012) 472-480.